J. Fluid Mech. (2024), *vol*. 981, A14, doi:10.1017/jfm.2024.22

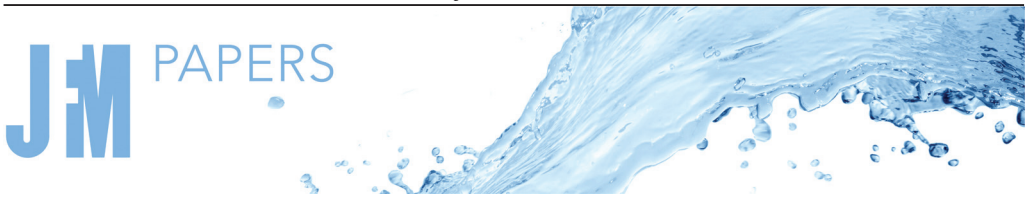

A shear stress parametrization for arbitrary wind farms in conventionally neutral boundary layers

Sebastiano Stipa[1],†, **D. Allaerts**[2] **and J. Brinkerhoff**[1]

[1]University of British Columbia–Okanagan Campus, Kelowna, BC V1V 1V7, Canada

[2]Faculty of Aerospace Engineering, TU Delft, 2629 HS Delft, The Netherlands

(Received 31 July 2023; revised 28 December 2023; accepted 29 December 2023)

In the context of large off-shore wind farms, power production is influenced greatly by the turbine array's interaction with the atmospheric boundary layer. One of the most influencing manifestations of such complex interaction is the increased level of shear stress observed within the farm. This leads to higher momentum fluxes that affect the wind speed at the turbine locations and in the cluster wake. At the wind farm entrance, an internal boundary layer (IBL) grows due to the change in effective roughness imposed by the wind turbines, and for large enough clusters, this can reach the unperturbed boundary layer height in what is referred to as the fully developed regime. Downwind, a second IBL starts growing, while the shear stress profile decays exponentially to its unperturbed state. In the present study, we propose a simple analytical model for the vertical profile of the horizontal shear stress components in the three regions identified above. The model builds upon the top-down model of Meneveau (*J. Turbul.*, vol. 13, 2012, N7), and assumes that the flow develops in a conventionally neutral boundary layer. The proposed parametrization is verified successfully against large-eddy simulations, demonstrating its ability to capture the vertical profile of horizontal shear stress, and its evolution both inside and downwind of the wind farm. Our findings suggest that the developed model can prove extremely useful to enhance the physical grounds on which new classes of coupled wind farm engineering models are based, leading to a better estimation of meso-scale phenomena affecting the power production of large turbine arrays.

Key words: boundary layer structure, atmospheric flows, turbulent mixing

† Email address for correspondence: sebstipa@mail.ubc.ca

1. Introduction

Wind energy is a crucial renewable energy source for decarbonizing the electricity grid. Investments are focusing on massive off-shore clusters made of increasingly large wind turbines (IRENA 2019). In this context, the wind farm interaction with the atmospheric boundary layer (ABL) has emerged as an increasingly important aspect to account for and model in order to yield accurate power predictions. Its existence uncovered new phenomena that conventional models either fail to capture, such as the wind deceleration upstream of a turbine cluster (Bleeg *et al.* 2018), or model only partially, such as farm-scale wake effects (Nygaard *et al.* 2022). The latter are produced by the interacting turbine wakes that merge eventually to form an extended region of reduced momentum downstream of the wind farm. This process, characterized by complex flow dynamics, cannot be described solely by a simple combination of individual wake deficits, but is rather affected by the intricate interplay of additional physical phenomena. First, vertical momentum flux is increased because of the added shear stress created by the wind turbines (Allaerts & Meyers 2017). Second, the wind farm can be seen as a step change in equivalent roughness (Calaf, Meneveau & Meyers 2010; Chamorro & Porté-Agel 2011), which leads to the formation of internal boundary layers (IBLs) that grow from the wind farm start and exit (Elliott 1958; Pendergrass & Arya 1984; Savelyev & Taylor 2005). Downstream, it is expected that wake evolution is affected by boundary layer internal stability and enhanced vertical momentum fluxes produced by the augmented shear stress. These are all topics of growing interest for the scientific community as more wind farms are constructed near pre-existing ones (Nygaard *et al.* 2020; Stieren & Stevens 2021).

While conventional wake models (Jensen 1983; Ainslie 1988; Bastankhah & Porté-Agel 2014; Niayifar & Porté-Agel 2016) look at only the turbine scale, efforts to include some of the large-scale physics have been attempted by Pedersen *et al.* (2022) with the introduction of the so-called turbulence-optimized park model. On the other hand, a new class of models has emerged, adopting a 'coupled' approach wherein conventional turbine-scale wake models are coupled suitably with additional sub-models aimed at capturing the meso-scale physics that is otherwise absent. This concept, introduced initially by Frandsen *et al.* (2006), was later refined by Stevens, Gayme & Meneveau (2015) as the coupled wake boundary layer model, in which the original top-down model of Calaf *et al.* (2010) was coupled with a wake model to enhance wind farm power predictions. The top-down model, obtained by balancing horizontally averaged momentum across the wind farm layer, provides an increased equivalent roughness length inside the wind farm, and postulates two equilibrium layers characterized by different values of friction velocities. Although its original formulation assumed a fully developed regime and infinitely large wind farms, the top-down model has been extended later by Meneveau (2012) to the wind farm entrance region, where an IBL grows due to the step change in equivalent roughness produced by the wind farm. This updated model was then used by Shapiro *et al.* (2019), and later by Starke *et al.* (2021), in their area-localized coupled model. Specifically, both studies apply the top-down model to arbitrary wind farm geometries. While technically the model's derivation justifies its application solely to infinite arrays in the fully developed regime, the authors contend that by considering results as locally averaged and ensuring a wind farm of sufficient size for this horizontal filtering to be meaningful, the top-down parametrization can be extended effectively to arbitrary layouts.

The coupling idea has also been used by Nishino & Dunstan (2020) to develop a two-scale momentum theory linking conventional momentum theory with the large-scale momentum balance above the wind farm layer. This was later extended by Kirby, Dunstan & Nishino (2023) to predict the power of large wind farms using the unperturbed shear

stress profile as input. Finally, Stipa *et al.* (2023*a*) introduced recently the multi-scale coupled model to capture global blockage and other free atmosphere stability effects on wind farm performance.

Focusing on the meso-scale side of the problem, it is clear that an accurate parametrization of the shear stress profile evolution within and past the wind farm is crucial to enhance predictions of momentum availability at the large scale. This would allow a more physics-based approach to model the turbulent mixing enhancement produced by wind farms within the coupled class of models. In the present study, we focus our attention on conventionally neutral boundary layers (CNBLs), where a stable free atmosphere characterized by a lapse rate γ and a strong inversion layer with temperature jump $\Delta\theta$ overtops a neutrally stratified layer in which turbulence develops capped by the inversion layer (Zilitinkevich *et al.* 2012). The wind profile of a CNBL differs from that of a truly neutral boundary layer where stratification is fully absent, in that a deviation from the standard law of the wall and the formation of a super-geostrophic jet have been observed (Kelly, Cersosimo & Berg 2019; Liu, Gadde & Stevens 2021).

On the other hand, the influence of internal ABL stability on the shear stress profile has been studied by Nieuwstadt (1983), who concluded that the vertical profile of shear stress magnitude approaches the classic linear shape

$$\tau/u^{*2} = 1 - z/H \tag{1.1}$$

(where H is the boundary layer height) for neutral or fully convective conditions, while in stable cases, it exhibits an upward concavity that increases with stability. In particular, Nieuwstadt (1984) modelled the stable, nocturnal boundary layer as

$$\tau/u^{*2} = (1 - z/H)^{3/2}. \tag{1.2}$$

In CNBLs, only the free atmosphere is thermally stratified, so turbulence develops mainly as in neutral conditions except close to the inversion layer, where buoyancy effects become important. As a consequence, as testified by the large-eddy simulations (LES) conducted by Allaerts & Meyers (2017), Abkar & Porté-Agel (2013) and Liu *et al.* (2021), the shear stress profile is almost linear in its lower part, and transitions smoothly to zero with a mild concavity close to H. Finally, when a wind farm is present within the boundary layer, the shear stress profile retains its self-similarity above the wind farm layer if non-dimensionalized with the friction velocity that characterizes the layer above the wind turbines, referred to as u^*_{hi} (Calaf *et al.* 2010; Kirby *et al.* 2023).

Building on the top-down model of Meneveau (2012), we propose here a simple analytical model for the horizontal shear stress components τ_{xz} and τ_{yz} around a large finite-size turbine array. The model is validated against data from LES, and captures the evolution of the horizontal shear stress components in three different flow regions, namely the developing region of the wind farm IBL, the fully developed region (if present), and the wind farm wake.

The present paper is organized as follows. The proposed shear stress model is described in § 2, while § 3 validates the model against LES data presented in Stipa *et al.* (2023*a*). Conclusions are finally drawn in § 4, together with notes on future work and the limitations of the present study.

2. Methodology

We assume that the background state existing without the wind farm corresponds to a CNBL of height H, i.e. with neutral stratification below a capping inversion layer centred

at H. Furthermore, we define h_{hub} and D as the average hub height and turbine diameter within the cluster, while z_0 is the unperturbed equivalent roughness height in the absence of any turbine. For simplicity, we assume that the wind is aligned with the x coordinate, while y corresponds to the spanwise direction. Wind farm entrance effects are modelled by considering an IBL of height δ_f that grows from the start of the wind farm (Chamorro & Porté-Agel 2011; Meneveau 2012) due to the change in roughness produced by the cluster. In addition, a second IBL, characterized by a height δ_w, grows from the wind farm exit due to the roughness transitioning back to z_0. Finally, similarly to Starke *et al.* (2021), we assume that the conditions at a given point exclusively depend on the upstream averaged planform wind farm thrust coefficient c_{ft}. This in turn depends on the rotor diameter, turbine C_T and spacings S_x and S_y, as detailed in § 2.1.

We subdivide the boundary layer structure into four vertically stacked layers, shown in figure 1(*a*). The 'low-stress layer' spans from z_0 to $h_{hub} - D/2$; the 'wind farm layer' spans from $h_{hub} - D/2$ to δ_w; the 'high-stress layer' spans from δ_w to δ_f; and the 'background stress layer' spans from δ_f to H. The vertical shear stress magnitude profile is assumed to be piecewise linear and continuous at each layer interface. This is a reasonable assumption for truly or conventionally neutral boundary layers, but may be revised in the future for internally stable ABLs where the background shear stress profile depicts an upward concavity (Nieuwstadt 1984). Analytical expressions within each layer are derived by exploiting the theory developed by Frandsen *et al.* (2006) and later refined by Calaf *et al.* (2010). Specifically, these authors introduced a relation for the increased wind farm equivalent roughness height $z_{0,hi}$, and postulated the existence of constant stress layers below and above the wind turbines, characterized by friction velocities u^*_{lo} and u^*_{hi}, respectively. The horizontal shear stress components τ_{xz} and τ_{yz} are obtained from the modelled profile of shear stress magnitude by assuming that the shear stress angle profile is unperturbed by the wind farm. Extension of such theory to the wind farm wake is done by assuming an exponential return of u^*_{lo} and u^*_{hi} to the unperturbed friction velocity u^*, resulting in a decay of the vertical shear stress profile to its unperturbed shape far downstream. A qualitative sketch of the model is given in figure 1. Note that the height of the wake boundary layer δ_w is constant and equal to $h_{hub} + D/2$ throughout the wind farm (figure 1*a*), while the wind farm boundary layer height δ_f is constant in the wind farm wake. In particular, if a fully developed regime is reached inside the wind farm, then δ_f coincides with the unperturbed boundary layer height H; otherwise, it is set to the value of δ_f obtained at the wind farm exit.

In our study, we consider H as constant, neglecting its potential growth from turbulent entrainment at the boundary layer's top and fluctuations caused by atmospheric gravity waves. While, notably, turbulent entrainment affects H if infinite wind farms are considered (Abkar & Porté-Agel 2013; Porté-Agel, Bastankhah & Shamsoddin 2020), its resulting growth rate leads to only marginal changes in H over the transit time of a flow particle through a wind farm of finite length. In this case, the more substantial contribution comes from interface waves within the inversion layer and atmospheric gravity waves in the free atmosphere. These waves induce both positive and negative displacements across the wind farm's length, potentially influencing pressure and velocity below the inversion and thereby impacting wind farm power dynamics (Lanzilao & Meyers 2023; Stipa *et al.* 2023*a*). Despite its influence on velocity, the inversion displacement caused by gravity waves remains minor compared to the unperturbed H, prompting its exclusion from our proposed parametrization.

Overall, the developed model has four free parameters, namely the two friction velocities u^*_{lo} and u^*_{hi}, together with the heights of the two IBLs generated by the step change

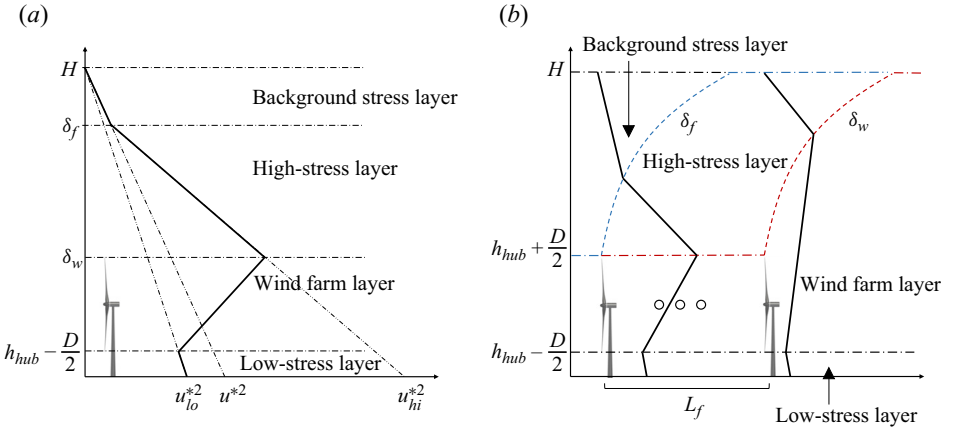

Figure 1. (*a*) Sketch of the proposed shear stress profile model inside the wind farm. (*b*) Qualitative evolution of the vertical profile of shear stress magnitude inside and downwind of the wind farm. Note that δ_w is constant and equal to $h_{hub} + D/2$ inside the wind farm.

in roughness, δ_f and δ_w, growing from the wind farm entrance and exit, respectively. Parametrization of these quantities in the wind farm and the wake regions is described in §§ 2.1 and 2.2.

2.1. *Wind farm parametrization*

Due to the presence of the wind turbines, the approaching flow experiences a sudden change in equivalent roughness length, which transitions from z_0 to $z_{0,hi}$. As a result, an IBL characterized by a height δ_f grows with increasing distance x from the wind farm entrance. At the same time, friction velocities u^*_{lo} and u^*_{hi} adjust to their fully developed values, obtained when $\delta_f = H$. Different expressions have been proposed for δ_f, obtained using both velocity and shear stress metrics. For instance, Shir (1972) and Allaerts & Meyers (2017), observed that shear stress adapts faster than velocity to a sudden increase in roughness. In the present study, the IBL height is identified as the vertical location where the relative difference between the actual and unperturbed shear stress magnitude vanishes, and it is modelled following Pendergrass & Arya (1984), who expressed δ_f as

$$\delta_f = \min\left[H, z_{tt} + 0.32 z_{0,hi}\left(\frac{d_f}{z_{0,hi}}\right)^{0.8}\right], \tag{2.1}$$

where z_{tt} is the average top-tip height, and d_f is the distance from the wind farm start. The increased equivalent roughness height is given by

$$z_{0,hi} = h_{hub}\left(1 + \frac{D}{2h_{hub}}\right)^{\beta} \exp\left[-\left(\frac{\widetilde{c_{ft}}}{2\kappa^2} + \left[\ln\left(\frac{h_{hub}}{z_0}\left(1 - \frac{D}{2h_{hub}}\right)^{\beta}\right)\right]^{-2}\right)^{-1/2}\right], \tag{2.2}$$

where $\beta = \nu^*_w/(1 + \nu^*_w)$ is evaluated using $\nu^*_w \approx 28\sqrt{0.5\widetilde{c_{ft}}}$ (see Calaf *et al.* (2010) for details). Note that δ_f, $z_{0,hi}$, β and ν^*_w are all functions of position $\boldsymbol{x}$, but such dependency has been dropped for ease of notation. The parameter $\widetilde{c_{ft}}$ (also a function of position)

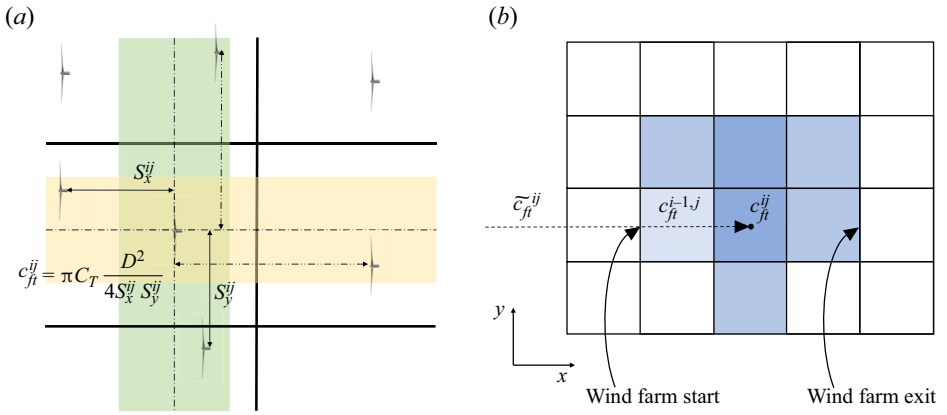

Figure 2. (*a*) Sketch of the turbine spacing evaluation algorithm. In yellow and green are the stripes to select those turbines that should be used for computing streamwise and spanwise spacing, respectively. (*b*) Sketch of the ray-casting procedure to evaluate $\widetilde{c_{ft}}^{ij}$ at the cell of interest from the c_{ft} field defined on the sampling grid. This procedure is also used to infer the start and ending coordinates of the wind farm.

can be evaluated by averaging the wind farm thrust coefficient per unit area c_{ft} upwind with respect to location $\boldsymbol{x}$ and along a streamline through the point of interest, assumed in the present study to be rectilinear. Following Starke *et al.* (2021), we argue that such an averaging procedure better represents the fact that the IBL height at any x depends on the thrust coefficient per unit area experienced up to that point rather than on its local value. In order to perform the averaging operation, c_{ft} is defined at every cell of a two-dimensional Cartesian sampling grid as

$$c_{ft}^{ij} = \pi C_T \frac{D^2}{4 S_x^{ij} S_y^{ij}}, \tag{2.3}$$

where C_T is the thrust coefficient of the closest turbine, while S_x^{ij} and S_y^{ij} are the streamwise and spanwise turbine spacings at a given cell. Their values are obtained as follows. First, for each turbine, we define x and y stripes characterized by a two diameters width, whose axis of symmetry passes through the turbine base location. Then streamwise and spanwise spacings S_x and S_y associated with the wind turbine of interest are found by looking for its closest rotor belonging to the x and y stripes, respectively (figure 2*a*). To transfer such information to the sampling grid, we first find the wind turbine closest to each grid cell, then set S_x^{ij} and S_y^{ij} to the values associated with the closest turbine. In doing so, if the closest turbine lies outside of the grid cell, then S_x^{ij} and S_y^{ij} are set to infinity, so that c_{ft}^{ij} approaches zero (no wind turbines are in the cell). The grid spacings along x and y are set to the maximum between S_x and S_y among all turbines in the cluster. This approach resembles that of Starke *et al.* (2021), who used a Voronoi tessellation that assigns a triangular grid cell to each wind turbine, but leaves the wind farm wake uncovered by the tessellation. Since in our approach we are interested in not only the shear stress within the wind farm but also its downstream evolution, a Cartesian grid is the simplest and most natural choice to achieve this objective.

Once c_{ft}^{ij} is known, the upwind-averaged $\widetilde{c_{ft}}^{ij}$ can be evaluated by casting a ray directed upwind from the cell centre of interest (figure 2*b*), and averaging c_{ft}^{ij} on the ray. In this regard, three cases are possible. If the query point is upwind of the wind farm, then $\widetilde{c_{ft}}^{ij}$ is

set to zero. If the query point is inside the wind farm, then $\widetilde{c_{ft}}^{ij}$ is set to the average c_{ft} on the ray from the wind farm start up to the query point. Finally, if the point lies within the wind farm wake, then $\widetilde{c_{ft}}$ is set to the average c_{ft} on a ray spanning the whole wind farm. In the latter case, the resulting $\widetilde{c_{ft}}$ corresponds to the value at the wind farm exit, used to compute u^*_{lo} and u^*_{hi} at the same location. Then an exponential decay will be applied to model a partial return of u^*_{lo} and u^*_{hi} to their equilibrium values (this is explained in more detail in § 2.2). To detect the point location with respect to the wind farm, we use the c_{ft} field itself. In fact, as it goes from zero to a positive value, query points will be inside the wind farm until c_{ft} goes back to zero. Conversely, after the latter condition is verified, points will be located in the wake. The same argument can be used to infer the distance of any given point $\boldsymbol{x}$ from the wind farm start or exit. Note that the above algorithm treats each ray – or streamwise stripe of cells – as if it were infinite in the spanwise direction, so that there is no mutual interaction between adjacent strips. Starke *et al.* (2021) made the same approximation, which is justified in our case by the fact that the proposed model already filters the actual shear stress profiles by smoothing the thrust coefficient per unit area over the Cartesian cells.

Once $z_{0,hi}$ and δ_f are known at any grid cell, friction velocities u^*_{lo} and u^*_{hi} can be evaluated as

$$u^*_{hi} = u^* \frac{\ln\left(\dfrac{\delta_f}{z_0}\right)}{\ln\left(\dfrac{\delta_f}{z_{0,hi}}\right)}, \tag{2.4}$$

$$u^*_{lo} = u^*_{hi} \frac{\ln\left[\dfrac{h_{ref}}{z_{0,hi}}\left(1+\dfrac{D}{2h_{ref}}\right)^{\beta}\right]}{\ln\left[\dfrac{h_{ref}}{z_0}\left(1-\dfrac{D}{2h_{ref}}\right)^{\beta}\right]}. \tag{2.5}$$

Finally, after having introduced $\tau_{w,lo} = u^{*2}_{lo}$, $\tau_{w,hi} = u^{*2}_{hi}$ and $\tau_{w,\infty} = u^{*2}$, the vertical profile of shear stress magnitude can be fully defined at every cell in each layer as

$$\tau_{lsl} = \tau_{w,lo}\left(1-\frac{h}{H}\right), \quad h \le z_{bt} \quad \text{(low-stress layer)}, \tag{2.6}$$

$$\begin{aligned}\tau_{wfl} = {} & \frac{h-z_{tb}}{z_{tt}-z_{tb}}\left[\tau_{w,lo}\left(\frac{z_{tb}}{H}-1\right)+\tau_{w,hi}\left(1-\frac{z_{tt}}{\delta_f}\right)+\tau_{w,\infty}\left(\frac{z_{tt}}{\delta_f}-\frac{z_{tt}}{H}\right)\right] \\ & + \tau_{w,lo}\left(1-\frac{z_{tb}}{H}\right), \quad z_{bt} < h \le \delta_w \quad \text{(wind farm layer)},\end{aligned} \tag{2.7}$$

$$\tau_{hsl} = \frac{h}{\delta_f}\left[\tau_{w,\infty}\left(1-\frac{\delta_f}{H}\right)-\tau_{w,hi}\right]+\tau_{w,hi}, \quad \delta_w < h \le \delta_f \quad \text{(high-stress layer)}, \tag{2.8}$$

$$\tau_{bsl} = \tau_{w,\infty}\left(1-\frac{h}{H}\right), \quad \delta_f < h \le H \quad \text{(background stress layer)}, \tag{2.9}$$

where z_{bt} and z_{tt} are the turbine bottom-tip and top-tip heights, respectively. The resulting profile, depicted in figure 1(*a*), is piecewise linear and continuous at the layer heights.

u_{ref} (m s^{-1})	h_{ref} (m)	θ_0 (K)	Δh (m)	$\Delta\theta$ (K)	γ (K km^{-1})	H (m)	f_c (s^{-1})	z_0 (m)
9.0	90	300	100	7.312–4.895	1	500	9.6057×10^{-5}	0.05

Table 1. Input parameters for the wind farm simulations.

Note that the background stress layer is present only in the developing region of the wind farm IBL, while it disappears once $\delta_f = H$. Conversely, the high-stress layer is non-existent at the wind farm start where $\delta_f = z_{tt}$.

2.2. *Wake parametrization*

At the wind farm exit, another discontinuity in roughness height is encountered from $z_{0,hi}$ to z_0. As a consequence, a second IBL will start growing, while u^*_{lo} and u^*_{hi} will return slowly to the unperturbed friction velocity u^* as

$$u^*_{hi} = [1 - \exp(-d_w/L)]u^* + \exp(-d_w/L)u^*_{hi,e}, \tag{2.10}$$

$$u^*_{lo} = [1 - \exp(-d_w/L)]u^* + \exp(-d_w/L)u^*_{lo,e}, \tag{2.11}$$

where d_w is the distance from the wind farm exit of the query point, $u^*_{hi,e}$ and $u^*_{lo,e}$ are the friction velocities obtained at the wind farm exit, and L is a length scale related to the turbulence decay. In the present study, we fix L to 5 km, which is expected to hold for neutral CNBLs and a background roughness close to the value reported in table 1. This provided the highest agreement with our LES results.

For instance, Cañadillas *et al.* (2020) developed an analytical model to predict velocity in the wake and used the time scale

$$T = \frac{\Phi(\xi)\, D^2}{\kappa u^* z_{hub}}, \tag{2.12}$$

where $\Phi(\xi)$ is the non-dimensional wind shear, a function of the Monin–Obukhov similarity parameter ξ inside the boundary layer (Stull 1988). One interesting aspect that can be observed is that the time scale for velocity recovery does not depend on the wind farm length. Moreover, as pointed out by Cañadillas *et al.* (2020), shear stress and velocity are tightly related in the wind farm wake, so the same finding can be expected for the recovery of shear stress. Specifically, while it is true that the wind farm length determines how much shear stress can evolve before leaving the cluster, its recovery is expected to depend only on general wind turbine characteristics, internal ABL stability and equivalent roughness height. However, as mentioned by Allaerts & Meyers (2017), shear stress adapts faster than velocity to changes in equivalent roughness. This can be observed also in Bastankhah *et al.* (2023) and may lead to a slightly different recovery time scale between these two quantities. Therefore, although in general we expect L to have a similar functional relationship with (2.12) – of course, after multiplying by a suitable mean advection velocity – this requires further investigation and has not been addressed in the present paper. Downstream of the wind farm, the IBL growth is approximated as

$$\delta_w = \min\left[H, z_{tt} + 0.32 z_0 \left(\frac{d_w}{z_0}\right)^{0.8}\right], \tag{2.13}$$

again following Pendergrass & Arya (1984). Its effect is to raise the top of the wind farm layer until it reaches the unperturbed boundary layer height H. In order to compute the

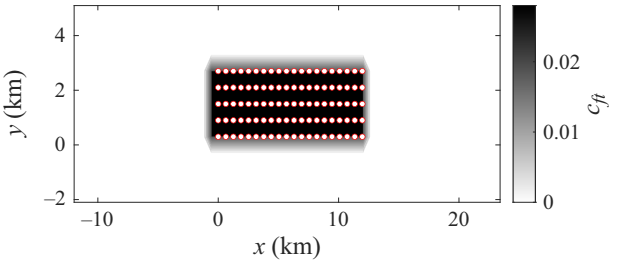

Figure 3. Contour of the c_{ft} field resulting from applying the algorithm presented in § 2.1. Red circles identify the wind turbine locations.

shear stress, (2.6)–(2.9) still hold upon substituting z_{tt} with δ_w, as the wind farm layer does not have a constant thickness downstream of the cluster (see figure 1*b*).

3. Results

In this section, we validate the proposed model for the vertical shear stress profile against LES conducted with TOSCA (Toolbox fOr Stratified Convective Atmospheres). TOSCA solves the incompressible Navier–Stokes equations, formulated in generalized curvilinear coordinates, exploiting the finite-volume method. Details about the code and its validation are provided in Stipa *et al.* (2023*b*). The two LES cases differ only in the prescribed capping inversion strength, and correspond to the subcritical and supercritical conditions presented in Stipa *et al.* (2023*a*). Our choice to vary the inversion strength is justified by results from Lanzilao & Meyers (2023), where $\Delta\theta$ emerges as the main parameter influencing wind farm flows under stratified free atmosphere, together with the lapse rate γ and inversion height H. The wind farm consists of 100 NREL 5 MW wind turbines (Jonkman *et al.* 2009), organized in 20 rows and 5 columns. Streamwise and spanwise turbine spacings are set to 630 m and 600 m, respectively. To prescribe a realistic turbulent inflow condition to the wind farm, we use the hybrid offline/concurrent precursor technique described in Stipa *et al.* (2023*b*). The offline precursor has been carried out for 100 000 s, while the successor phase of the analysis lasted for 20 000 s. Statistics are gathered for the last 15 000 s of simulation. Input parameters for the ABL are reported in table 1, where θ_0 and Δh are the ground potential temperature and inversion width, respectively, that are used together with $\Delta\theta$, γ and H to initialize the background potential temperature profile with the model proposed by Rampanelli & Zardi (2004). The parameter u_{ref} is the average wind at h_{ref} (chosen as the wind turbine hub height), while z_0 is the equivalent roughness length. Further details on the simulation set-up are given in Stipa *et al.* (2023*a*).

Regarding the shear stress model, we calculate the unperturbed shear stress angle profile from the LES, but this can also be evaluated using e.g. the model proposed by Nieuwstadt (1983). Moreover, wind turbine C_T resulting from the LES is fairly constant throughout the wind farm as all turbines operate below rated conditions. Hence for the shear stress model we assume $C_T = 0.85$ for all turbines in the present study, which results in a constant c_{ft} field equal to 0.028 throughout the wind farm. We highlight that the procedure presented in § 2.1 to compute the c_{ft} field does not impose any restriction on the wind farm geometry, except that the wind farm has to be large enough to produce perturbations in shear stress when this is averaged around the location of interest. Figure 3 shows the c_{ft} field corresponding to the wind farm object of the present study. Specifically, this is finite in both the spanwise and streamwise directions.

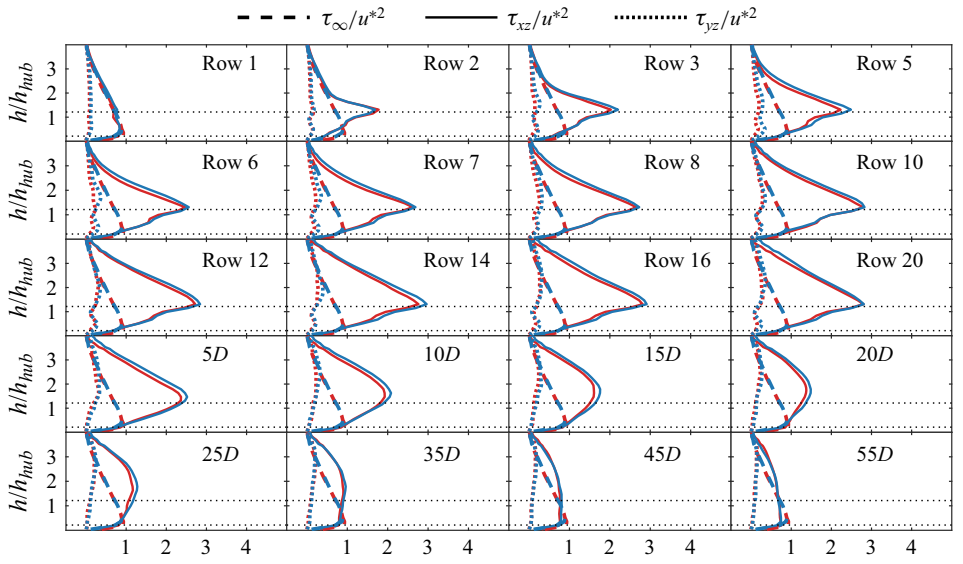

Figure 4. Comparison of shear stress profiles between the two LES for different locations inside the wind farm (identified by the row number) and in the wind farm wake (identified by the distance in diameters from the wind farm exit). Red indicates $\Delta\theta = 7.312$; blue indicates $\Delta\theta = 4.895$; horizontal dotted lines indicate top and bottom turbine tip heights.

Figure 4 compares profiles of τ_{xz} and τ_{yz} from the two LES. Data have been spanwise-averaged from $y = 0$ to $y = 3000$, corresponding to the wind farm spanwise envelope. Surprisingly, the variation in inversion strength between the two cases does not impact the shear stress profile evolution within or beyond the wind farm. This suggests that also free atmosphere stratification aloft, typically weaker than the stability found in the inversion layer, might not affect the shear stress disturbances caused by the wind farm. In light of these observations, while stability within the inversion and in the free atmosphere have large implications in the wind speed dynamics (Allaerts & Meyers 2017; Lanzilao & Meyers 2023; Stipa *et al.* 2023*a*), we argue that the physics of shear stress perturbations seems mainly confined to the boundary layer flow, thus justifying the absence of a free atmosphere parametrization in the proposed model. Conversely, internal ABL stability is expected to play an important role, and this is a subject for further investigation. Looking at figure 4, it can be seen how the peak in τ_{xz} is located at z_{tt} inside the wind farm, while it shifts upwards in the wind farm wake, where the shear stress returns slowly to its equilibrium value. Finally, the growth of δ_f is clearly visible, as the height at which the local profile differs from the free-stream increases with downstream distance from the wind farm entrance.

Figure 5 compares profiles of τ_{xz} and τ_{yz} resulting from the proposed model against their LES predictions from the two simulations. Also in this case, LES data have been averaged along the spanwise direction from $y = 0$ to $y = 3000$. For reference, we also show in each plot the free-stream shear stress magnitude profile τ_∞, evaluated from LES. It can be noticed how the model predictions agree well with the LES results, both inside and downstream of the wind farm for the two simulated cases. Moreover, the assumption that the wind farm does not perturb the initial shear stress angle profile significantly is verified, as both profiles of τ_{xz} and τ_{yz} predicted by the model are in strong agreement with the LES data, especially in the fully developed region. Here, the maximum value of τ_{xz} is around three times $\tau_{w,\infty}$, meaning that vertical momentum fluxes are strongly enhanced by

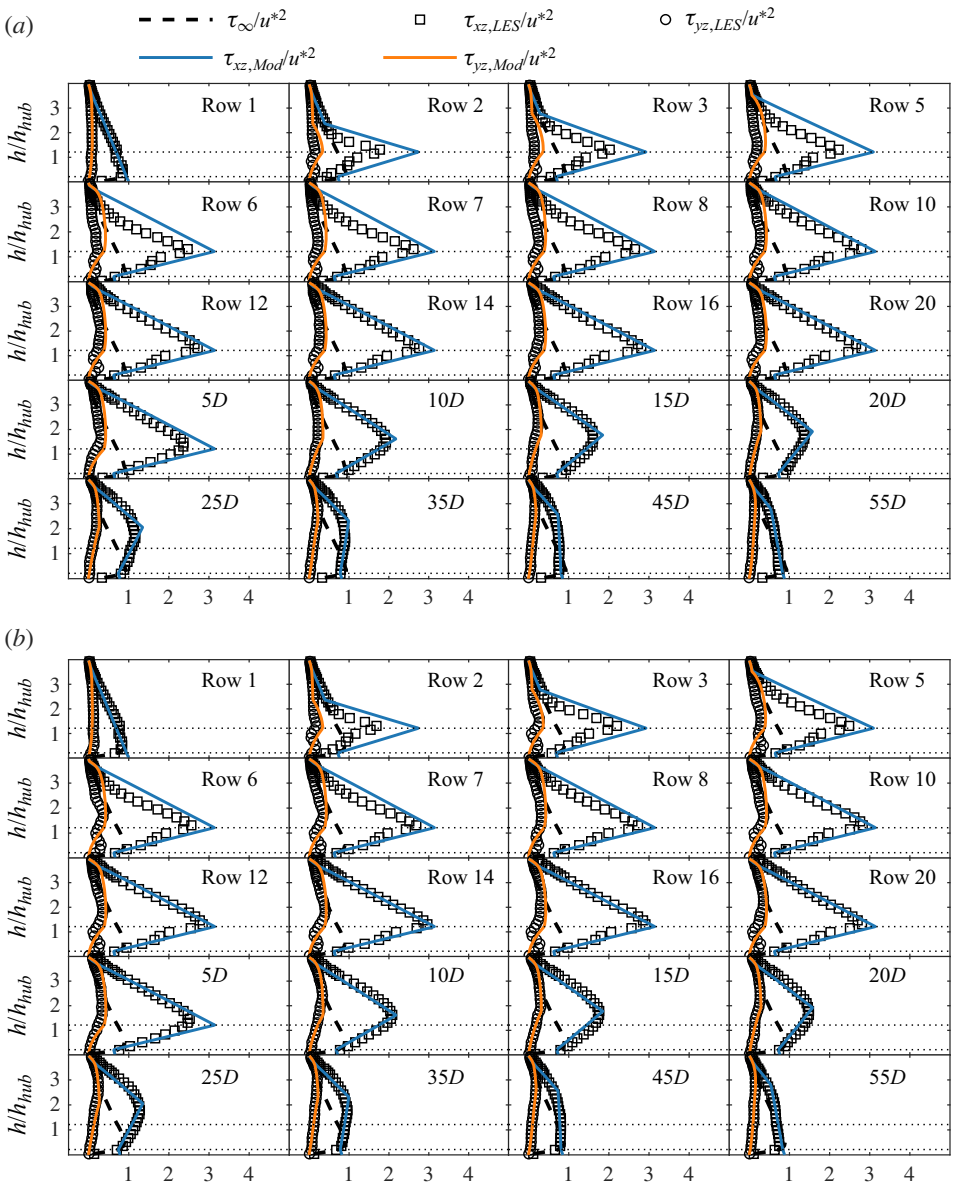

Figure 5. Comparison between the proposed model and LES results for different locations inside the wind farm (identified by the row number) and in the wind farm wake (identified by the distance in diameters from the wind farm exit) for (*a*) $\Delta\theta = 7.312$ and (*b*) $\Delta\theta = 4.895$. Horizontal dotted lines indicate top and bottom turbine tip heights.

the presence of the wind farm. In the developing region, especially where δ_f approaches H, the shear stress profile evaluated from the LES exhibits an upward concavity close to H, slightly disagreeing with the piecewise linear approximation. This effect could be due to non-negligible thermal and non-equilibrium effects that may affect the shear stress profile near H in the region where the flow transitions to a fully developed regime. Nevertheless, the piecewise linear assumption describes satisfactorily the features of the shear stress profile in all regions on the flow, with the highest agreement found in the wind farm wake and in the fully developed region.

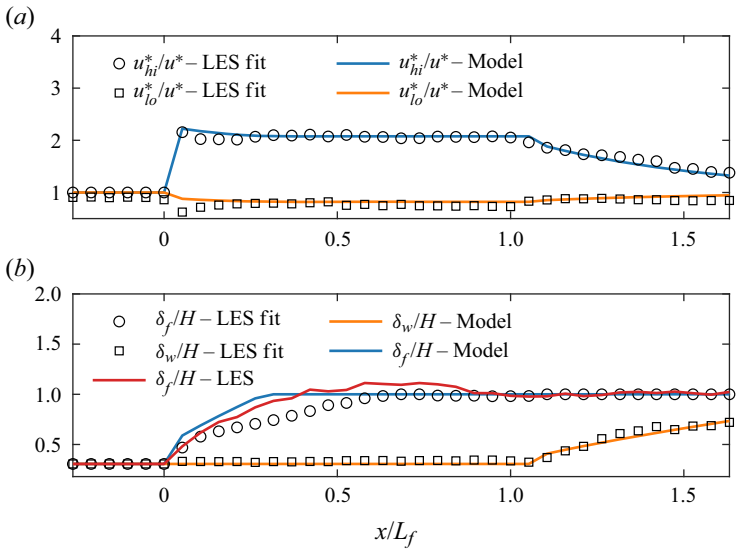

Figure 6. Comparisons between values of (*a*) u^*_{hi} and u^*_{lo}, and (*b*) δ_f and δ_w, obtained using the formula of Pendergrass & Arya (1984) and as a result of fitting LES results with the assumed shear stress model shape in a least squares sense (LES fit). The red line in (*b*) corresponds to δ_f evaluated from LES data using the criterion explained in the text (LES).

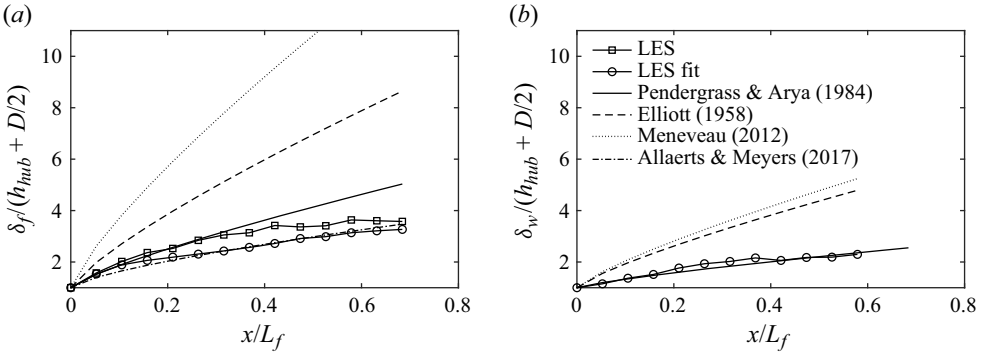

Figure 7. Comparison of (*a*) wind farm IBL δ_f and (*b*) wake IBL δ_w obtained using different analytical formulas and as calculated by fitting LES data with the assumed shape for the vertical profile of shear stress magnitude (LES fit). For δ_f, results obtained with the criterion explained in the text (LES) and from the Allaerts & Meyers (2017) formula are also shown.

In order to assess the accuracy of the methodology used to compute u^*_{lo}, u^*_{hi}, δ_f and δ_w, we performed a least squares fit of the shear stress magnitude profile obtained from the LES with its piecewise linear shape assumed in the proposed model. In particular, we left u^*_{lo}, u^*_{hi}, δ_f and δ_w free to be determined by the least squares fit operation. Results for the $\Delta\theta = 7.312$ case are shown in figure 6, where we report u^*_{lo}, u^*_{hi}, δ_f and δ_w evaluated using both the least squares fit and the equations reported in § 2. The same analysis for the $\Delta\theta = 4.895$ case points to similar conclusions, hence it is not reported. Referring to figure 6, while very good agreement can be found in the friction velocities u^*_{lo} and u^*_{hi}, the least squares fit predicts a slower growth of the wind farm IBL than (2.1). This can be confirmed also by looking at the developing region in figure 5, i.e.

from row 1 to row 8. Conversely, good agreement is found when analytical predictions of δ_f are compared against data obtained from LES by using the following criterion. At each streamwise location, we first look for the height where the difference between the actual and unperturbed stress is less than 5 % of u^{*2}. Then δ_f is extrapolated as the height where such difference is zero. Such a criterion, depicted in red in figure 6, predicts a faster growth of δ_f if compared with the least squares fit. A possible reason is that within the developing region, the shear stress profile in the high-stress layer is not strictly linear but instead features the upward concavity mentioned above. As a consequence, minimizing the least squares error within the whole layer or adopting the proposed criterion locally yields differences in the shear stress slope, reflected in slightly distinct δ_f predictions. Conversely, the analytical growth of the wake IBL given by (2.13) follows closely the least squares fit obtained in the wind farm wake, supporting our choice to model the upward shift of the wind farm layer top. This allows the model to capture the upward displacement of the shear stress peak located initially at z_{tt} at the wind farm exit.

Finally, figure 7 compares different analytical formulations for the IBL growth (see Savelyev & Taylor (2005) for a review) against LES data already shown in figure 6. Also in this case, we show only data from the case characterized by $\Delta\theta = 7.312$. All studies approximate δ as

$$\frac{\delta}{z_{0,D}} = \frac{\delta(0)}{z_{0,D}} + A\left(\frac{x}{z_{0,D}}\right)^{0.8}, \tag{3.1}$$

where $z_{0,D}$ is the roughness height downstream of the discontinuity. In particular, it can be noticed how, for both δ_f and δ_w, the formulas of Elliott (1958) and Meneveau (2012) predict a faster IBL growth than what is observed in our numerical simulations, as they assume $A = 0.75 + 0.03\ln(z_{0,D}/z_{0,U})$ and $A = 1.0$, respectively, where $z_{0,U}$ is the roughness height upwind of the discontinuity. For this reason, we used the analytical formulation of Pendergrass & Arya (1984), who estimated $A = 0.32$. The same observation was also made by Allaerts & Meyers (2017), who estimated δ_f as $\delta_f(0) + 0.57x^{0.74}$. For instance, this result agrees well with the wind farm IBL predicted by fitting the LES data with the shear stress model shape, suggesting that further research may be needed to fully understand wind farm IBL growth.

4. Conclusions

In the present study, we introduced an analytical model to predict the vertical profiles of shear stress magnitude for the flow around a finite-size wind farm in a conventionally neutral boundary layer. The model has been validated against LES results, and proved to capture accurately the growth of the wind farm IBL, the shear stress profile in the developing and fully developed region, as well as the return to equilibrium of the shear stress components in the wind farm wake, where the growth of a second IBL is observed. The suite of LES cases revealed that the shear stress is not influenced by the strength of the inversion layer, suggesting that its shape and evolution may not be influenced by free atmosphere stratification. Moreover, the assumption that the vertical profile of shear stress angle is negligibly perturbed by the wind farm is well verified if stress components obtained from the LES are compared against the shear stress magnitude from the model, projected with the unperturbed angle profile resulting from the LES. The model features four free parameters, namely the height of the two IBLs within and downstream of the wind farm, δ_f and δ_w, respectively, and the friction velocities u^*_{lo} and u^*_{hi} in the layers of constant stress postulated by Calaf *et al.* (2010), below and above the wind turbines, respectively.

While u^*_{lo} and u^*_{hi} are found analytically using the top-down model (Meneveau 2012), δ_f and δ_w are evaluated using the formula proposed by Pendergrass & Arya (1984), which predicts a slower IBL growth than the expression from Meneveau (2012). Ultimately, these four parameters define the vertical profile of shear stress magnitude, whose shape is postulated. To assess the accuracy of the top-down model, we fitted the shear stress profiles obtained from LES with the shape assumed by the model, and similar values for u^*_{lo}, u^*_{hi}, δ_f and δ_w have been found.

Further research is needed to assess the dependency of the length scale L used to control the turbulence decay in the wind farm wake, in particular studying its dependence on boundary layer internal stability. In the latter case, the assumed piecewise shape of the shear stress profile should also be verified. Moreover, to assess the accuracy of the model with different levels of background shear stress, we plan to extend the suite of validation to different values of equivalent roughness length.

Overall, we believe that the developed shear stress model provides an important advancement in modelling the increase in shear stress within large finite-size wind farms, enabling a better understanding of its effects by providing a simple yet comprehensive formulation to model vertical momentum fluxes at a given height within the boundary layer.

Funding. The present study is supported by UL Renewables and the Natural Science and Engineering Research Council of Canada (NSERC) through Alliance grant no. 556326. Computational resources provided by the Digital Research Alliance of Canada (www.alliancecan.ca) and Advanced Research Computing at the University of British Columbia (www.arc.ubc.ca) are gratefully acknowledged.

Declaration of interests. The authors report no conflict of interest.

Author ORCIDs.
Sebastiano Stipa https://orcid.org/0009-0001-2540-3098;
D. Allaerts https://orcid.org/0000-0002-8758-3952;
J. Brinkerhoff https://orcid.org/0000-0003-4106-9293.

References

Abkar, M. & Porté-Agel, F. 2013 The effect of free-atmosphere stratification on boundary-layer flow and power output from very large wind farms. *Energies* **6**, 2338–2361.

Ainslie, J.F. 1988 Calculating the flowfield in the wake of wind turbines. *J. Wind Engng Ind. Aerodyn.* **27** (1), 213–224.

Allaerts, D. & Meyers, J. 2017 Boundary-layer development and gravity waves in conventionally neutral wind farms. *J. Fluid Mech.* **814**, 95–130.

Bastankhah, M., Mohammadi, M.M., Lees, C., Diaz, G.P.N., Buxton, O. & Ivanell, S. 2023 A fast-running physics-based wake model for a semi-infinite wind farm. *J. Fluid Mech.* (submitted) arXiv:2309.08711.

Bastankhah, M. & Porté-Agel, F. 2014 A new analytical model for wind-turbine wakes. *Renew. Energy* **70**, 116–123.

Bleeg, J., Purcell, M., Ruisi, R. & Traiger, E. 2018 Wind farm blockage and the consequences of neglecting its impact on energy production. *Energies* **11** (6), 1609.

Calaf, M., Meneveau, C. & Meyers, J. 2010 Large eddy simulation study of fully developed wind-turbine array boundary layers. *Phys. Fluids* **22** (1), 015110.

Cañadillas, B., *et al.* 2020 Offshore wind farm wake recovery: airborne measurements and its representation in engineering models. *Wind Energy* **23** (5), 1249–1265.

Chamorro, L. & Porté-Agel, F. 2011 Turbulent flow inside and above a wind farm: a wind-tunnel study. *Energies* **4**, 1916–1936.

Elliott, W.P. 1958 The growth of the atmospheric internal boundary layer. *Eos, Trans. Am. Geophys. Union* **39** (6), 1048–1054.

FRANDSEN, S., BARTHELMIE, R., PRYOR, S., RATHMANN, O., LARSEN, S., HØJSTRUP, J. & THØGERSEN, M. 2006 Analytical modelling of wind speed deficit in large offshore wind farms. *Wind Energy* **9** (1–2), 39–53.

IRENA 2019 Future of wind: deployment, investment, technology, grid integration and socio-economic aspects (a global energy transformation paper). *Tech. Rep*. International Renewable Energy Agency, Abu Dhabi.

JENSEN, N.O. 1983 A note on wind generator interaction. *Risø-M* 2411. Risø National Laboratory.

JONKMAN, J.M., BUTTERFIELD, S., MUSIAL, W. & SCOTT, G. 2009 Definition of a 5 MW reference wind turbine for offshore system development. National Renewable Energy Laboratory (NREL).

KELLY, M., CERSOSIMO, R.A. & BERG, J. 2019 A universal wind profile for the inversion-capped neutral atmospheric boundary layer. *Q. J. R. Meteorol. Soc.* **145** (720), 982–992.

KIRBY, A., DUNSTAN, T. & NISHINO, T. 2023 An analytical model of momentum availability for predicting large wind farm power. *J. Fluid Mech*. **976**, A24.

LANZILAO, L. & MEYERS, J. 2023 A parametric large-eddy simulation study of wind-farm blockage and gravity waves in conventionally neutral boundary layers. *J. Fluid Mech*. **979**, A54.

LIU, L., GADDE, S.N. & STEVENS, R.J.A.M. 2021 Universal wind profile for conventionally neutral atmospheric boundary layers. *Phys. Rev. Lett.* **126**, 104502.

MENEVEAU, C. 2012 The top-down model of wind farm boundary layers and its applications. *J. Turbul.* **13**, N7.

NIAYIFAR, A. & PORTÉ-AGEL, F. 2016 Analytical modeling of wind farms: a new approach for power prediction. *Energies* **9**, 741.

NIEUWSTADT, F.T.M. 1983 On the solution of the stationary, baroclinic Ekman-layer equations with a finite boundary-layer height. *Boundary-Layer Meteorol.* **26** (4), 377–390.

NIEUWSTADT, F.T.M. 1984 The turbulent structure of the stable, nocturnal boundary layer. *J. Atmos. Sci.* **41** (14), 2202–2216.

NISHINO, T. & DUNSTAN, T.D. 2020 Two-scale momentum theory for time-dependent modelling of large wind farms. *J. Fluid Mech.* **894**, A2.

NYGAARD, N.G., POULSEN, L., SVENSSON, E. & GRØNNEGAARD PEDERSEN, J. 2022 Large-scale benchmarking of wake models for offshore wind farms. *J. Phys.: Conf. Ser.* **2265**, 022008.

NYGAARD, N.G., STEEN, S., POULSEN, L. & PEDERSEN, J.G. 2020 Modelling cluster wakes and wind farm blockage. *J. Phys.: Conf. Ser.* **1618**, 062072.

PEDERSEN, J.G., SVENSSON, E., POULSEN, L. & NYGAARD, N.G. 2022 Turbulence optimized Park model with Gaussian wake profile. *J. Phys.: Conf. Ser.* **2265**, 022063.

PENDERGRASS, W. & ARYA, S.P.S. 1984 Dispersion in neutral boundary layer over a step change in surface roughness – I. Mean flow and turbulence structure. *Atmos. Environ.* **18** (7), 1267–1279.

PORTÉ-AGEL, F., BASTANKHAH, M. & SHAMSODDIN, S. 2020 Wind-turbine and wind-farm flows: a review. *Boundary-Layer Meteorol.* **174** (1), 1–59.

RAMPANELLI, G. & ZARDI, D. 2004 A method to determine the capping inversion of the convective boundary layer. *J. Appl. Meteorol.* **43**, 925–933.

SAVELYEV, S. & TAYLOR, P. 2005 Internal boundary layers: I. Height formulae for neutral and diabatic flows. *Boundary-Layer Meteorol.* **115**, 1–25.

SHAPIRO, C.R., STARKE, G.M., MENEVEAU, C. & GAYME, D.F. 2019 A wake modeling paradigm for wind farm design and control. *Energies* **12** (15), 2956.

SHIR, C.C. 1972 A numerical computation of air flow over a sudden change of surface roughness. *J. Atmos. Sci.* **29** (2), 304–310.

STARKE, G.M., MENEVEAU, C., KING, J.R. & GAYME, D.F. 2021 The area localized coupled model for analytical mean flow prediction in arbitrary wind farm geometries. *J. Renew. Sustain. Energy* **13** (3), 033305.

STEVENS, R.J.A.M., GAYME, D.F. & MENEVEAU, C. 2015 Coupled wake boundary layer model of wind-farms. *J. Renew. Sustain. Energy* **7** (2), 023115.

STIEREN, A. & STEVENS, R. 2021 Evaluating wind farm wakes in large eddy simulations and engineering models. *J. Phys.: Conf. Ser.* **1934**, 012018.

STIPA, S., AJAY, A., ALLAERTS, D. & BRINKERHOFF, J. 2023*a* The multi-scale coupled model: a new framework capturing wind farm–atmosphere interaction and global blockage effects. *Wind Energy Sci. Discuss.* **2023**, 1–44.

STIPA, S., AJAY, A., ALLAERTS, D. & BRINKERHOFF, J. 2023*b* TOSCA – an open-source finite-volume LES environment for wind farm flows. *Wind Energy Sci. Discuss.* **2023**, 1–41.

STULL, R.B. 1988 *An Introduction to Boundary Layer Meteorology*, 1st edn. Springer.

ZILITINKEVICH, S.S., TYURYAKOV, S., TROITSKAYA, YU.I. & MAREEV, E.A. 2012 Theoretical models of the height of the atmospheric boundary layer and turbulent entrainment at its upper boundary. *Izv. Atmos. Ocean. Phys.* **48**, 133–142.